IEEE Access
Multidisciplinary | Rapid Review | Open Access Journal

Received July 30, 2020, accepted August 16, 2020, date of publication September 22, 2020, date of current version October 14, 2020.

Digital Object Identifier 10.1109/ACCESS.2020.3025935

A Common-Mode Noise Suppression Filter for Gigahertz Differential Signals Based on Substrate Integrated Waveguide Resonators

XIAO-LAI LI, GUOMIN YANG, (Senior Member, IEEE), AND QINZHUO CHEN
Key Laboratory for Information Science of Electromagnetic Waves (MoE), Fudan University, Shanghai 200433, China

Corresponding author: Guomin Yang (guominyang@fudan.edu.cn)

This work was supported in part by the National Natural Science Foundation of China under Grant U1637213, and in part by the National Key Research and Development Program of China under Grant 2017YFA0700203.

ABSTRACT A common-mode noise suppression filter for microstrip differential lines based on substrate integrated waveguide resonator (SIWR) is proposed in this article. The proposed common-mode filter (CMF) consists of cascaded SIWR units with different size. The equivalent characteristic impedance circuit model of the proposed CMF is given to predict the common-mode suppression characteristics by introducing the spectral domain approach (SDA). Simulated results show that the common-mode noise is decreased more than 35 dB from 4.5 GHz to 11.4 GHz, and −30 dB rejection band is obtained in the frequency band of 4.3-15 GHz. Moreover, the insertion loss and the group delay in the frequency domain show that there is little degradation for differential signals. In the time domain, 86.5% amplitude suppression of common-mode noise is achieved. In addition, the eye diagrams in the time domain are investigated to explain the effectiveness of the proposed CMF and indicate that the CMF can maintain the differential signal integrity. The prototype is fabricated to verify the validity of the proposed structure, and the measurement results show good agreement with the simulation results.

INDEX TERMS Common-mode filter (CMF), high-speed differential signals, spectral domain approach (SDA), substrate integrated waveguide resonator (SIWR), signal integrity.

I. INTRODUCTION

Differential signals have played an important role in the signal transmission of modern high-speed circuits. Common applications include serial advanced technology attachment III (SATA III), high definition multimedia interface (HDMI) and universal serial bus (USB) devices [1]. The advantages of using differential signals include lower levels of unintentional radiation, reduced susceptibility to external interference and more accurate system timing sequence compared with traditional single-ended signals. However, it is inevitable that common-mode noise will be generated due to non-ideal asymmetric differential lines, which could be caused by fabrication tolerance, circuit layout or coupled spurious signals. When common-mode noises pass through the interconnection in the system packaging structure of high-speed circuits, it will cause serious electromagnetic radiation, and affect the signal integrity (SI) and power integrity (PI) of the circuits. Therefore, how to design CMF with high performances, which can not only suppress common-mode noise, but also ensure effective and lossless transmission of differential signals, has become one of the hotspots that need to be studied urgently in high-speed interconnection.

There have been some methods for designing CMF. The common-mode choke [2]–[4] using ferrite material is employed to suppress the common-mode noise of differential signals. However, it is not suitable for gigahertz differential signals. Low-temperature co-fired ceramic (LTCC) filters [5] also can be used to reduce the common-mode noise, but it may increase the fabrication complexity and costs.

Recently, there are some reported CMFs in the differential signals based on defected ground structure (DGS) [6]–[8]. DGS method can realize good performances of suppressing common-mode noise in a wide frequency band by interfering the common-mode current on the ground. The fractional bandwidth of the stopband over 15 dB can

The associate editor coordinating the review of this manuscript and approving it for publication was Bo Pu.

This work is licensed under a Creative Commons Attribution 4.0 License. For more information, see https://creativecommons.org/licenses/by/4.0/

reach 87% and 118% in literatures [6] and [7], respectively. However, DGS method cannot be implemented in multilayer structure because the performance will deteriorate if there is a metal plane under DGS structure [1]. Electromagnetic bandgap (EBG) [9]–[18] is another common CMF structure which can be used in multilayer structure. In [9] and [10], EBG filters are introduced to reduce the common-mode noises of differential striplines. Traditional EBG structure of mushroom and planar EBG are implemented for the suppression of common-mode noise of differential signals in [12] and [13], respectively. Literature [15] has reported a removable CMF based on EBG. Nevertheless, EBG filter is limited in applications because it usually cannot realize a wideband common-mode noise reduction. In addition, there are some literatures with a combination of aforementioned methods. Common-mode noise suppression below −20 dB is obtained in the frequency band of 3.3-7 GHz with EBG and DGS in [19]. In [20], [21], the fractional bandwidth of 34% and 98% in common-mode rejection are achieved using complementary split ring resonators (CSRR) and double slit complementary split ring resonator (S-DBCSRR) based on DGS, respectively. Chen *et.al* presented a CMF based on varactor-loaded slot-ring resonator on the ground [22]. Artificial transmission lines are used to reject dual-band common-mode noise in [29]. Similarly, they are not appropriate for multilayer structures due to the defected ground.

Besides, open stub grounded resonators are employed for rejecting the common-mode radiation and electromagnetic interference in [23]. In the same way, a simple CMF using quarter-wavelength open stub resonator is investigated comprehensively in literature [1], and the ultra-wideband common-mode noise rejection can be obtained using cascaded quarter-wavelength resonators with different size. Furthermore, [24] and [25] proposed the CMFs with periodically corrugated reference plane (PCRP) and inter-digital fingers for the common-mode noise rejection in high-speed differential signals, respectively. Common-mode noise rejection is realized for balanced bandpass filters in multilayer liquid crystal polymer technology by using folded stepped impedance resonator (SIR) and the proposed 4-cell common-mode rejection structure in [30].

In this article, a common-mode noise suppression filter for high-speed differential signals based on substrate integrated waveguide resonator (SIWR) is presented. To obtain an ultra-wideband common-mode noise suppression, SIWR units with different size are cascaded. The fractional bandwidth of rejection band for the common-mode noise below −35 dB can reach over 86% and the common-mode noise suppression less than −30 dB can be obtained in the frequency band of 4.3-15 GHz. For further investigating the characteristic of the proposed CMF, the equivalent characteristic impedance circuit model of the proposed CMF is given to explain the principle by using the SDA, and the group delay in the frequency domain and the eye diagram in the time domain are studied to prove the effectiveness of the proposed structure. The detailed structure and equivalent circuit analysis of the proposed CMF unit are presented in section II. In section III, the characteristic is analyzed for the cascaded CMF units with different size. Then, the designed prototype is fabricated and measured, and the measurement results are discussed and compared with the simulated results in section IV, followed by conclusions in section V.

II. COMMON-MODE FILTER UNIT DESIGN AND ANALYSIS

A. CMF UNIT STRUCTURE DESIGN AND WORKING PRINCIPLE

The schematic model of the proposed CMF unit is presented in Fig. 1. The CMF unit consists of three layers. The differential microstrip lines are on the top layer. The SIWR structure is placed under the differential microstrip lines, and three columns of vias are used to connect the second layer and the third layer (the ground). The dielectric substrate FR4 ($\varepsilon_r = 4.4$ and $\tan\delta = 0.02$) has a thickness of 1.1 mm and the SIWR structure has a height of 1 mm.

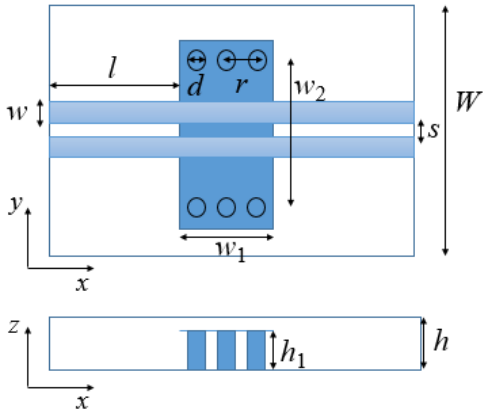

FIGURE 1. Schematic of the proposed CMF unit.

As is known, most of differential signals propagate close to the plane that differential microstrip lines are located due to reverse voltages, while most of common-mode noises propagate between the differential microstrip lines and the ground. Based on these propagation characteristics for differential signals and common-mode signals, a substrate integrated waveguide structure is introduced to realize the common-mode noise suppression. SIWR structure has the similar characteristics as rectangle waveguides resonators, and the standing wave pattern will be formed inside when the working frequency is equal to the resonant frequency of resonators. Therefore, the common-mode noises will be rejected around the resonant frequency of SIWR because most of common-mode noises pass through the SIWR structure. On the other hand, there is little impact on the differential signals due to that most of waves propagate close to the plane that the differential microstrip lines are located for differential signals. Fig. 2 (a) and (b) show the electric field distribution of the proposed CMF at the common-mode resonant frequency of 8.9 GHz for even-mode and odd-mode, respectively. It can be seen that TE_{110} mode is excited when even-mode signals

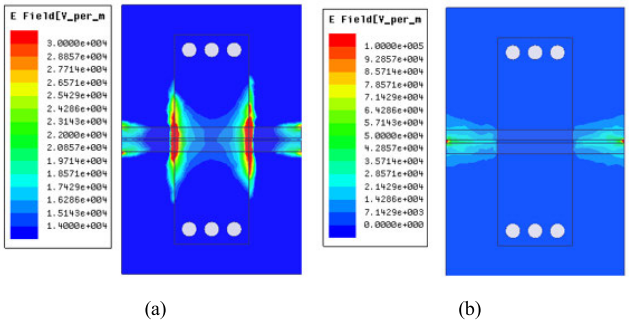

FIGURE 2. The electric field distribution of the proposed CMF unit at 8.9 GHz (a) odd-mode (b) even-mode.

propagate through the SIWR, while there are almost no interactions between SIW CMF and the coupled microstrip lines when differential signals are propagating.

B. THE EQUIVALENT CIRCUIT OF CMF

Fig. 3 (a) and (b) show the equivalent circuits of the proposed CMF unit for the odd-mode and even-mode, respectively. In the case of odd-mode, it is equal to place a perfect electric wall in the middle of differential microstrip lines so that short-circuit is formed here, which indicates that the second layer has the same potential as the ground. Therefore, for the odd-mode case, the impedance Z_{0o} and Z_{0ol} will be equivalent to the odd-mode impedances of coupled microstrip lines with the height of 0.1 mm and 1.1 mm, respectively. Similarly, for the even-mode case, corresponding open-circuit will appear in the middle of differential microstrip lines where a perfect magnetic wall is placed. The odd-mode and even-mode characteristic impedances of coupled microstrip lines are presented in equations (1a) and (1b).

$$Z_{ce} = \frac{Z_c\sqrt{\varepsilon_{re}/\varepsilon_{re}^e}}{1 - Q_4 Z_c\sqrt{\varepsilon_{re}}/377} \tag{1a}$$

$$Z_{co} = \frac{Z_c\sqrt{\varepsilon_{re}/\varepsilon_{re}^o}}{1 - Q_{10} Z_c\sqrt{\varepsilon_{re}}/377} \tag{1b}$$

$$L \approx \mu_0 \frac{h_1}{2\pi}\left[\ln\left(\frac{2h_1}{\frac{d}{2}} + \sqrt{1+\left(\frac{2h_1}{\frac{d}{2}}\right)^2}\right) - \sqrt{1+\left(\frac{\frac{d}{2}}{2h_1}\right)^2} + \frac{\frac{d}{2}}{2h_1} + \frac{1}{4}\right] \tag{2}$$

where ε_{re} and Z_c are the static effective dielectric constant and the characteristic impedance of single microstrip of width W, respectively. ε_{re}^e and ε_{re}^o denote effective dielectric constants for even and odd modes, respectively [31]. The values of Q_4 and Q_{10} are given in literature [31].

C. CHARACTERISTIC IMPEDANCE OF BROADSIDE-COUPLED LINES

As shown in Fig. 3 (b), in the even-mode case, the interaction between the coupled microstrip lines and CMF can be represented by a broadside-coupled lines with one open-end. For obtaining the characteristic impedance of broadside-coupled lines in the equivalent circuit, spectral domain approach (SDA) is used here. It should be noted that the vias are not taken into account when using the SDA, as seen in Fig. 4, which is because we use the inductor L in the equivalent circuit of Fig. 3(b) to represent the effect of vias. The details of SDA was presented in [33], so we only give the essential steps here.

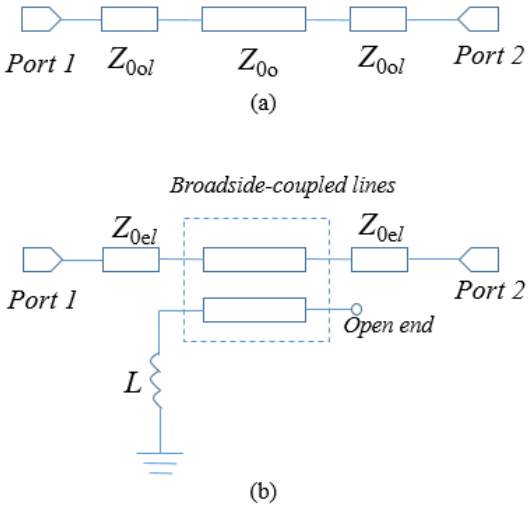

FIGURE 3. The equivalent circuit of the proposed CMF unit (a) odd-mode (b) even-mode.

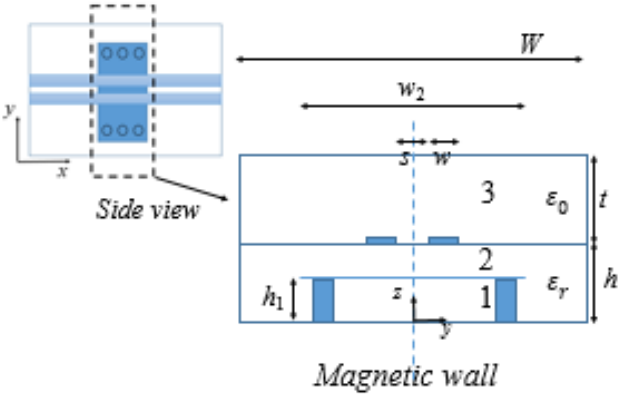

FIGURE 4. The side view of the proposed CMF unit for even-mode case.

The first step is to impose the boundary conditions at the interfaces along the z-direction in the space domain. We designate three regions, $0 < z < h_1$, $h_1 < z < h$, and $h < z < h + t$, corresponding to the index 1, 2 and 3 in Fig. 4, then the interface conditions to be satisfied can be expressed

as follows:

$$\varphi_1(y, h_1) = \varphi_2(y, h_1) \qquad 0 < y < W/2 \tag{3a}$$

$$\varphi_1(y, h_1) = \begin{cases} V_2, 0 < y < w_2/2 \\ \varphi_0(y), w_2/2 < y < W/2 \end{cases} \tag{3b}$$

$$\varepsilon_r \frac{\partial \varphi_2}{\partial z}\bigg|_{z=h_1} - \varepsilon_r \frac{\partial \varphi_1}{\partial z}\bigg|_{z=h_1} = \begin{cases} -\dfrac{\rho_s(y)}{\varepsilon_0}, 0 < y < \dfrac{w_2}{2} \\ 0, \dfrac{w_2}{2} < y < \dfrac{W}{2} \end{cases} \tag{3c}$$

$$\varphi_2(y, h) = \varphi_3(y, h) \quad 0 < y < W/2 \tag{4a}$$

$$\varphi_2(y, h_1) = \begin{cases} V_1, \dfrac{s}{2} < y < \dfrac{s}{2} + w \\ v(y), 0 < y < \dfrac{s}{2}, \dfrac{s}{2} + w < y < \dfrac{W}{2} \end{cases} \tag{4b}$$

$$\frac{\partial \varphi_3}{\partial z}\bigg|_{z=h} - \varepsilon_r \frac{\partial \varphi_2}{\partial z}\bigg|_{z=h} = \begin{cases} -\dfrac{\rho(y)}{\varepsilon_0}, \dfrac{s}{2} < y < \dfrac{s}{2} + w \\ 0, 0 < y < \dfrac{s}{2}, \dfrac{s}{2} + w < y < \dfrac{W}{2} \end{cases} \tag{4c}$$

where $\varphi_i(y, z)$, $i = 1, 2, 3$ denote the potentials in three regions, $\rho(y)$ and $\rho_s(y)$ represent the unknown charge distributions on the upper strip and lower strip, respectively. In addition, $v(y)$ and $\varphi_0(y)$ are unknown potential distributions at the interfaces.

Then the expressions (3a)-(3c) and (4a)-(4c) are transformed in the spectral domain by using Fourier transforms. On the other hand, when Fourier transformed, the Laplace equation for φ becomes:

$$\frac{d^2\tilde{\varphi}}{dz^2} - \hat{k}_n^2 \varphi = 0 \tag{5a}$$

$$\hat{k}_n = \frac{(n - \frac{1}{2})}{\frac{W}{2}}\pi \tag{5b}$$

And the solutions of (5a) in each region are

$$\tilde{\varphi}_1(n, z) = A_n sinh\hat{k}_n z \tag{6a}$$

$$\tilde{\varphi}_2(n, z) = B_n^s sinh\hat{k}_n(z - b) + B_n^c cosh\hat{k}_n(z - b) \tag{6b}$$

$$\tilde{\varphi}_3(n, z) = C_n sinh\hat{k}_n(h + t - z) \tag{6c}$$

Next, we substitute the expressions (6a)-(6c) into the transformed expressions in the spectral domain of (3a)-(3c) and (4a)-(4c), and express A_n, B_n^s, B_n^c, and C_n in terms of $\tilde{\rho}$ and $\tilde{\rho}_s$. The following equations will obtained

$$\tilde{G}_{11}\left(\hat{k}_n\right)\tilde{\rho}\left(\hat{k}_n\right) + \tilde{G}_{12}\left(\hat{k}_n\right)\tilde{\rho}_s\left(\hat{k}_n\right) = \tilde{\varphi}_{V_2} + \tilde{\varphi}_0 \tag{7a}$$

$$\tilde{G}_{21}\left(\hat{k}_n\right)\tilde{\rho}\left(\hat{k}_n\right) + \tilde{G}_{22}\left(\hat{k}_n\right)\tilde{\rho}_s\left(\hat{k}_n\right) = \tilde{\varphi}_{V_1} + \tilde{v} \tag{7b}$$

where

$$\tilde{G}_{11} = \frac{1}{\Delta}(\coth\hat{k}_n h_1 + \coth\hat{k}_n(h - h_1)) \tag{8a}$$

$$\tilde{G}_{12} = \tilde{G}_{21} = \frac{1}{\Delta}\frac{1}{\sinh\hat{k}_n(h - h_1)} \tag{8b}$$

$$\tilde{G}_{22} = \frac{1}{\Delta}(\frac{1}{\varepsilon_r}\coth\hat{k}_n t + \coth\hat{k}_n(h - h_1)) \tag{8c}$$

$$\Delta = \varepsilon_0\hat{k}_n\left[\varepsilon_r\left(\coth\hat{k}_n h_1 * \coth\hat{k}_n(h - h_1)\right) + 1) + \coth\hat{k}_n t(\coth\hat{k}_n(h - h_1) + \coth\hat{k}_n h_1)\right] \tag{8d}$$

We expand unknown $\tilde{\rho}$ and $\tilde{\rho}_s$ in terms of linear combinations of known sets of basis functions as

$$\tilde{\rho}\left(\hat{k}_n\right) = \sum_{k=1}^{K} a_k \tilde{\rho}_k\left(\hat{k}_n\right) \tag{9a}$$

$$\tilde{\rho}_s\left(\hat{k}_n\right) = \sum_{m=1}^{M} b_m \tilde{\rho}_{sm}\left(\hat{k}_n\right) \tag{9b}$$

Finally, we can derive the following system of linear equations by applying Galerkin's method along with Parseval's relation.

$$\sum_{k=1}^{K} K_{ik}^{11}\left(\hat{k}_n\right) a_k + \sum_{m=1}^{M} K_{im}^{12}\left(\hat{k}_n\right) b_m = P_i, \quad i = 1, 2, \ldots, K \tag{10}$$

$$\sum_{k=1}^{K} K_{jk}^{21}\left(\hat{k}_n\right) a_k + \sum_{m=1}^{M} K_{jm}^{22}\left(\hat{k}_n\right) b_m = Q_j, \quad j = 1, 2, \ldots, M \tag{11}$$

where

$$K_{ik}^{11}\left(\hat{k}_n\right) = \sum_{n=1}^{\infty} \tilde{\rho}_i\left(\hat{k}_n\right)\tilde{G}_{11}\left(\hat{k}_n\right)\tilde{\rho}_k\left(\hat{k}_n\right) \tag{12a}$$

$$K_{im}^{12}\left(\hat{k}_n\right) = \sum_{n=1}^{\infty} \tilde{\rho}_i\left(\hat{k}_n\right)\tilde{G}_{12}\left(\hat{k}_n\right)\tilde{\rho}_{sm}\left(\hat{k}_n\right) \tag{12b}$$

$$K_{jk}^{21}\left(\hat{k}_n\right) = \sum_{n=1}^{\infty} \tilde{\rho}_{sj}\left(\hat{k}_n\right)\tilde{G}_{21}\left(\hat{k}_n\right)\tilde{\rho}_k\left(\hat{k}_n\right) \tag{12c}$$

$$K_{jm}^{22}\left(\hat{k}_n\right) = \sum_{n=1}^{\infty} \tilde{\rho}_{sj}\left(\hat{k}_n\right)\tilde{G}_{22}\left(\hat{k}_n\right)\tilde{\rho}_{sm}\left(\hat{k}_n\right) \tag{12d}$$

$$P_i = \frac{W}{4}V_1\int_{\frac{s}{2}}^{\frac{s}{2}+w} \rho_i(y)dy \tag{13a}$$

$$Q_j = \frac{W}{4}V_2\int_{0}^{\frac{w_2}{2}} \rho_{sj}(y)dy \tag{13b}$$

where $\tilde{\rho}_i$ and $\tilde{\rho}_{sj}$ are the basis functions, here we select the Chebyshev's polynomials of the first kind [34] as the basis functions taking the edge effect into consideration. V_1 and V_2 represent the known potential on the upper strip and lower strip, respectively. To obtain accurate characteristic impedance, we need to set W and t infinity because our proposed structure is not the shielded structure as the literature [33] mentioned. Then the quasi-static capacitance per unit length for c-mode (the upper and lower strips are excited by equal potential, $V_1 = V_2 = 1$) and π-mode (the upper and lower strips are excited by opposite potential,

$V_1 = -V_2 = 1$) can be obtained by solving the equation (14).

$$C = \frac{4}{W}\sum_{k=1}^{K} a_k P_k \tag{14}$$

Finally, the characteristic impedances of equivalent circuit for even-mode case are computed by the following the equations [33]:

$$Z = Z_{air}\sqrt{\frac{C_{air}}{C}} \tag{15a}$$

$$Z_{air} = \frac{1}{cC_{air}} \tag{15b}$$

where c denotes the light velocity in free space, C_{air} is the line capacitance per unit length for the hypothetical problem for which $\varepsilon_r = 1$ in the same structure.

Consider one CMF unit where the geometry parameters w, w_1, w_2, s, d, r, l and W are 0.35 mm, 2.5 mm, 6 mm, 0.1 mm, 0.5 mm, 0.8 mm, 1.75 mm and 10 mm, respectively. Corresponding odd-mode and even-mode characteristic impedances Z_{0o}, Z_{0o_l}, Z_{0e_l} for the equivalent circuit are 28.4 Ω, 44.3 Ω and 166.8 Ω, respectively, by using equation (1a) and (1b). And c-mode and π-mode characteristic impedances for the broadside-coupled lines are 17.7 Ω and 122.8 Ω by using abovementioned SDA method, while the inductor L is approximately equal to 0.45 nH by using the equation (2) [32]. The proposed CMF unit is simulated with the software of CST Microwave Studio, and Fig. 5 depicts the comparison of the full-wave and equivalent circuit results for the CMF unit, which shows a good agreement.

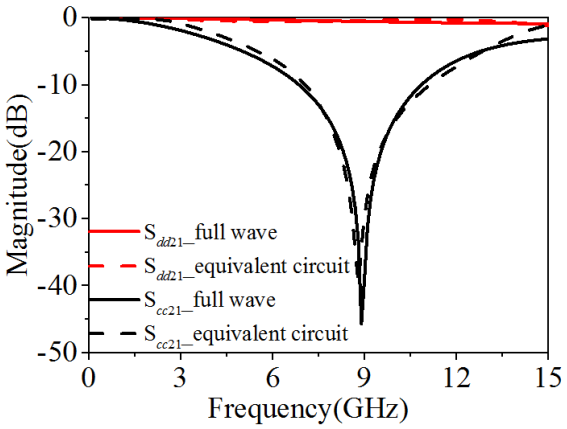

FIGURE 5. The comparisons of the full-wave and equivalent circuit results for the CMF unit.

D. PARAMETERS ANALYSIS

Fig. 6 presents the insertion loss of common-mode signals when the CMF unit includes one, two or three columns of vias, respectively. It is evident that the common-mode noise suppression becomes better with the increase of column number, here, we select three columns of vias for the CMF unit.

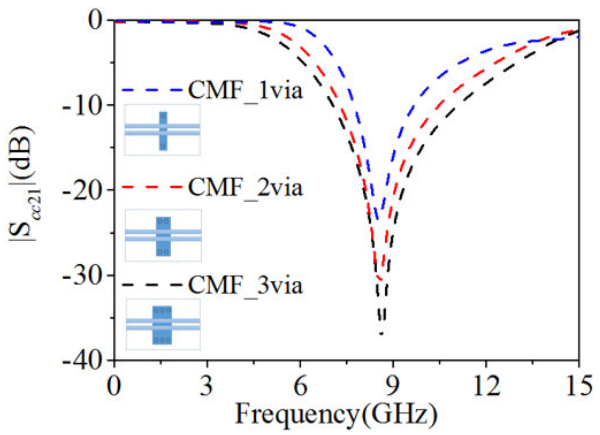

FIGURE 6. The insertion loss of common-mode signals when the CMF unit includes one, two or three columns of vias.

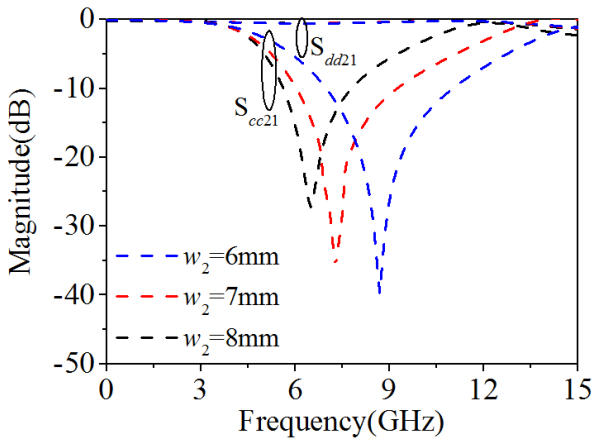

(a)

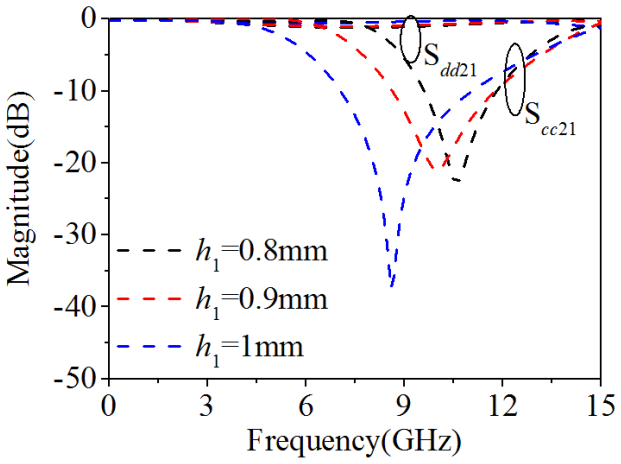

(b)

FIGURE 7. The insertion losses of differential and common-mode signals when the values of (a) w_2 are 6 mm, 7 mm and 8 mm while h_1 is 1mm (b) h_1 are 0.8 mm, 0.9 mm and 1 mm while w_2 is 6mm.

Fig. 7 (a) and (b) show the insertion loss of the differential and common-mode signals with the different values of w_2 and h_1, respectively. It can be observed that the resonant

frequency point shifts to lower frequency with the increase of the variables w_2 or h_1. Moreover, the common-mode noise suppression depth will be smaller when the value of h_1 decreases, therefore, the height of SIWR structure is set to 1 mm. The equations of the CMF unit resonant frequency are summarized for predicting the common-mode noise rejection characteristic in advance:

$$f \approx \frac{1}{2w_e\sqrt{\varepsilon\mu}}\left(0.3\ln\left(\frac{1}{h_1}\right)-1.321\right) \tag{16}$$

$$w_e = w_2 - 1.08\frac{d^2}{r}+0.1\frac{d^2}{w_2} \tag{17}$$

where ε and μ denote the permittivity and permeability of the substrate, respectively, and w_e is the equivalent width of the SIW structure [26].

III. WIDEBAND CMF ANALYSIS

For obtaining wideband common-mode noise suppression, the cascaded CMF units with different resonant frequencies of common-mode is an effective solution [27].

A. TWO CASCADED CMF UNITS ANALYSIS

Fig. 8 shows the simulated insertion loss of differential signals and common-mode noise with two cascaded CMF units, and it can be clearly seen that the common noise suppression bandwidth is broaden when two CMF units with different SIWR width are cascaded. Besides, the effects of the gap between two CMF units on the common-mode noises rejection are depicted. The gap must be large enough to allow the common-mode signals current to return through SIWR structure so that the larger depth of common-mode rejection can be achieved [1]. As shown in Fig. 8, when the gap exists, the suppression of common-mode noises is better than no gap, but the suppression characteristic is not changed much when the value of g is larger than 0.2 mm. Accordingly, the value of g is set to 0.2 mm. Moreover, the comparison of the equivalent circuit results and the full-wave simulation results for two cascaded CMF units is presented in Fig. 8, which shows a good agreement.

On the other hand, the insertion loss of differential signals is less than 1.2 dB up to 10.5 GHz as depicted in Fig. 8. Moreover, to keep good signal integrity for the differential-mode signals, in addition to small insertion loss, the group velocity is also a very important indicator [6]. Fig. 9 depicts the group delay comparisons with and without two cascaded common-mode filter units, and it can be seen that there are almost no effects on the group delay characteristic with the addition of the two-unit CMF. Therefore, signal integrity of differential signals is preserved.

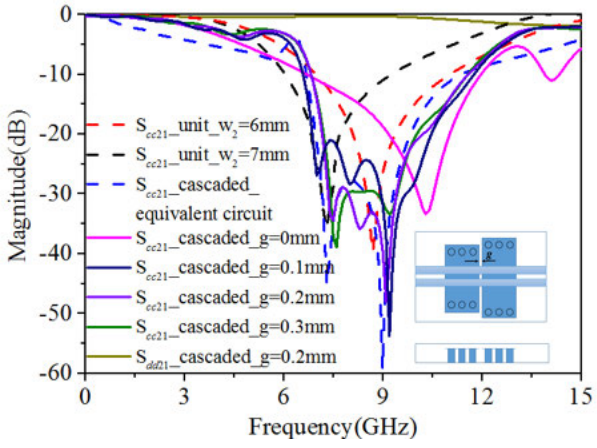

FIGURE 8. The simulated insertion loss of the two-unit CMF with different values of g.

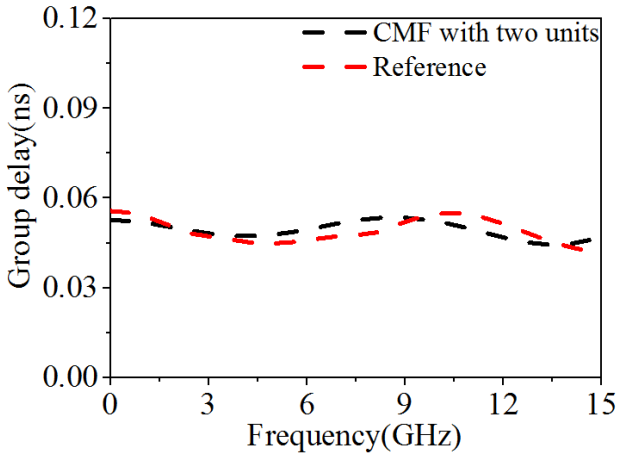

FIGURE 9. The simulated group delay comparisons with and without two cascaded CMF units.

B. ULTRA-WIDEBAND CMF ANALYSIS IN FREQUENCY DOMAIN

As shown in Fig. 10, eleven CMF units with different SIWR widths are cascaded to realize an ultra-wideband common-mode noise suppression. The values of eleven CMF units width are from 4 mm to 14 mm. Fig. 11 presents the insertion loss comparisons of differential and common-mode signals with and without the wideband CMF. We can see that the common-mode noise rejection below −35 dB is achieved from 4.5 GHz to 11.4 GHz, and the fractional bandwidth of rejection band for the common-mode noises below -30 dB can

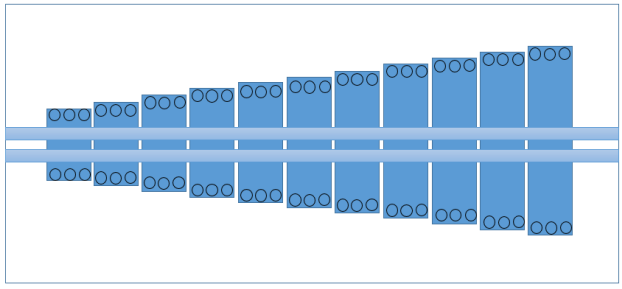

FIGURE 10. The schematic of the proposed ultra-wideband CMF.

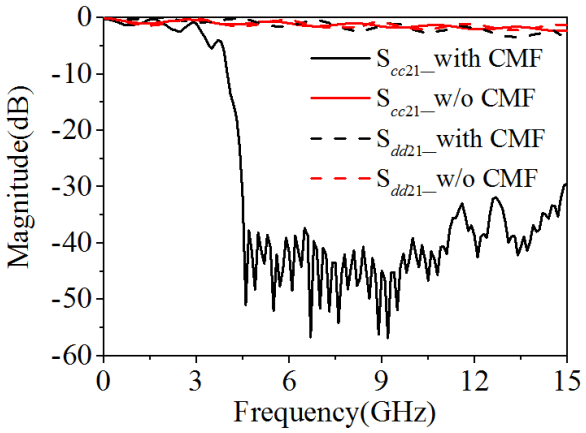

FIGURE 11. The simulated insertion loss comparisons of differential and common-mode signals with and without CMF.

reach over 110%. For the differential signals, it can be seen that the insertion loss is less than 4.2 dB up to 15 GHz and there is almost no degradation compared with the reference board without CMF structure. The group delay comparisons for differential signals with and without the wideband CMF are depicted in Fig. 12. The group delays of differential signals of the reference board and that of CMF board with eleven SIW units are approximately 0.235 ns and 0.245 ns, respectively, at the central frequency of 7.5 GHz, which indicates that a good signal integrity of the differential signals is maintained because of small insertion loss and group velocity for differential signals when they pass through the ultra-wideband CMF.

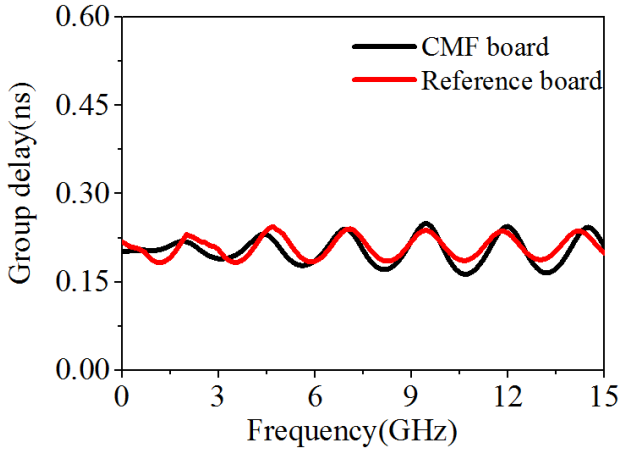

FIGURE 12. The simulated group delay comparisons for differential signals with and without ultra-wideband CMF.

C. ULTRA-WIDEBAND CMF ANALYSIS IN TIME DOMAIN

To verify the common-mode suppression characteristic of CMF in the time domain, a signal skew is created by designing a delay line of 4 mm [6], as shown in Fig. 13. Fig. 14 (a) and (b) show the common-mode and differential-mode voltage comparisons received at Port 2 when

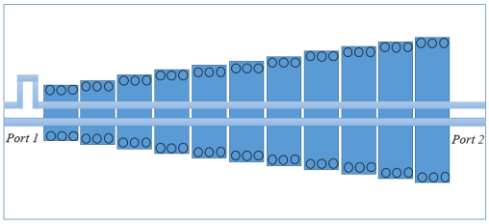

FIGURE 13. The schematic of the proposed ultra-wideband CMF with the time skew introduced.

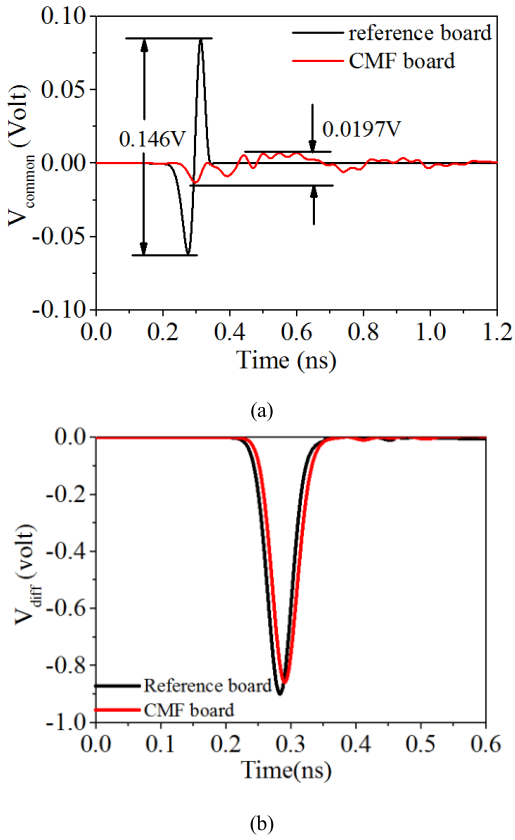

FIGURE 14. The simulated voltage comparisons received at Port 2 when differential-mode signals are excited at Port 1 with and without CMF. (a) common-mode (b) differential-mode.

differential-mode signals are excited at Port 1 with the reference board and CMF board, respectively. The common-mode noise is defined as half of the sum of voltages received at two output ports of differential traces [6]. Therefore, in the ideal case, the common-mode noise will not be excited due to that voltages received at two output ports have equal amplitude and inverse phase. However, the common-mode noise will be produced due to the change of amplitude and phase of voltages received when the signal skew is introduced. Fig. 14 (a) depicts that the peak-to-peak common-mode voltages of 0.146 V and 0.0197V are obtained, respectively, using the reference board and CMF board. Approximately 86.5% amplitude common-mode noise suppression is realized. For differential signals in the time domain, it can be seen that

two curves almost overlap each other, which means that the signal integrity of differential signals is retained. It can be explained that most of waves propagate close to the plane that differential microstrip lines are located for differential signals.

Fig. 15 (a) and (b) present the simulated eye diagrams of differential signals at data ratio of 10 Gb/s with the reference board and CMF board, respectively. The maximum eye height, maximum eye width and jitter are three important indicators to evaluate the quality of eye diagrams [6], and they are given in Table 1 for the CMF board and the reference board. It can be seen that the larger eye width and height are obtained with the CMF board, while there is smaller jitter than the reference board, which verifies that the signal integrity of differential signal is preserved when the CMF is introduced.

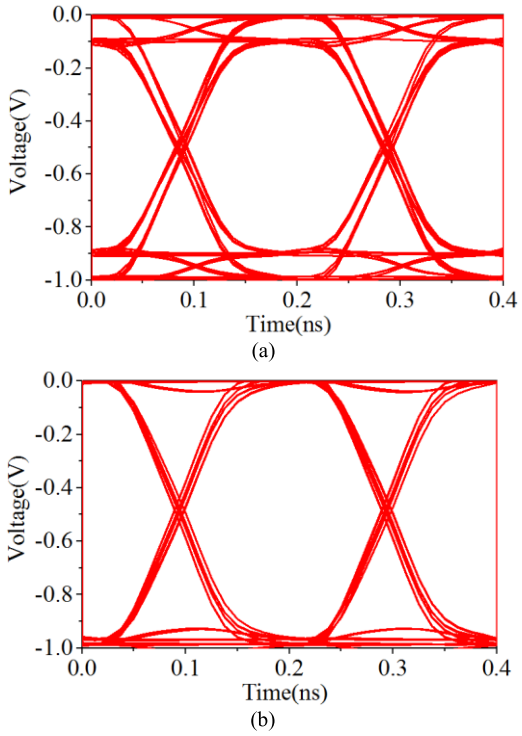

FIGURE 15. The simulated eye diagrams of differential signals at data ratios of 10 Gb/s with (a) reference board (b) CMF board.

IV. FABRICATION AND MEASUREMENTS

In order to validate the performance of the proposed common-mode noise suppression filter, the proposed prototype is fabricated as shown in Fig. 16. The prototype was fabricated using printed circuit board technology. The proposed structure comprises of top differential microstrip lines, a substrate with buried SIWR structure, and a metal ground. The substrate used here is FR4 ($\varepsilon_r = 4.4$ and $\tan\delta = 0.02$) with a thickness of 1.1 mm. The thickness of top metal patches and ground is 0.035 mm. It is worth noting that four right-angle bent patches are introduced to connect with differential microstrip lines for measuring the fabrication using SMAs. In addition, the right-angled triangles are removed

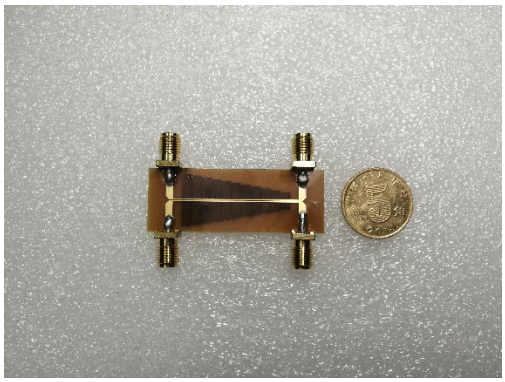

FIGURE 16. The fabricated sample of the proposed CMF.

at right-angled bends to decrease the losses that the bend discontinuity introduces [28].

Two ports of a vector network analyzer (Agilent N5227A) are connected with fabricated prototype, while another two ports of the fabrication are connected with 50 Ω matching loads to measure the characteristic in frequency domain. Fig. 17 shows the simulated and measured result comparisons of differential-mode and common-mode signals, and it can be seen that the common-mode stopband below −25 dB is achieved from 4.4 GHz to 14.4 GHz, while the measured insertion loss of differential signals is less than 4.7 dB up to 15 GHz. The main reason that insertion loss increases compared with the simulated results without right-angled bends but with CMF may attribute to the attenuation of differential signals at the right-angles bends, which can be

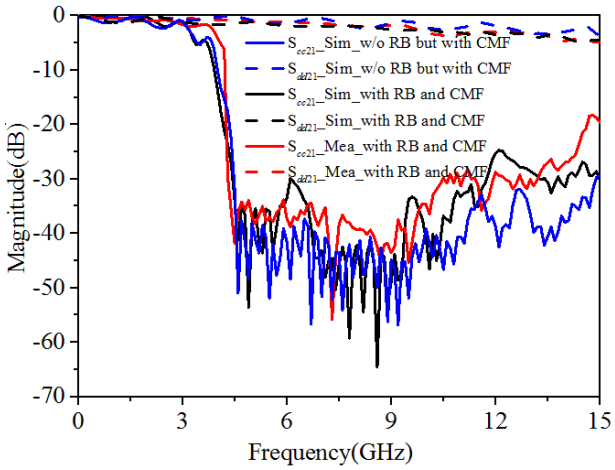

FIGURE 17. The simulated and measured results comparisons of (a) common-mode (b) differential-mode signals (RB: right-angled bends).

TABLE 1. Eye diagram parameter comparisons.

Parameters	Reference board	CMF board
Eye height	0.704 V	0.85 V
Eye width	0.187 ns	0.191 ns
Jitter	0.0138 ns	0.005 ns

TABLE 2. Comparison of our work with previous works.

Ref.	Method	Size ($\lambda_e \times \lambda_e$)	CMS (dB)	FB (GHz)	Fractional bandwidth	IL (dB)
[1]	Quarter-wavelength resonator	N/A	-20	3.7-7.3	65.5%	4.48
[6]	DGS	0.44×0.44	-10	3.8-9.7	87%	3
[7]	DGS	1.35×1.35	-15	3.2-12.4	117.9%	N/A
[18]	EBG	N/A	-15	1.75-2.75	44%	0.9
[19]	DGS+EBG	1.16×0.12	-15	3.3-8	80%	1.5
[20]	DS-CSRR	0.64×0.13	-20	1.16-1.85	41%	N/A
[21]	S-DBCSRR	0.43×0.15	-20	1.52-4.07	92%	0.8
[24]	PCRP	N/A	-10	5.3-10.4	65%	4.8
[30]	SIR	0.88×0.38	-20	3.2-5.4	50%	N/A
[35]	Periodic structure	1.66×0.75	-55	6.7-7.3	8.6%	2
This work	SIWR	1.01×0.48	-25	4.4-14.4	106.4%	4.7

FB: frequency band
CMS: common-mode suppression.
IL represents the insertion loss of differential signals.

proved by the good agreement between the simulated and measured results with right-angled bends and CMF. On the other hand, fabrication tolerance also may cause the increase of the insertion loss.

To measure the common-mode noises suppression property in time domain, arbitrary waveform generator (Tektronix 7122C) and digital serial analyzer (Tektronix 71604) are used, as shown in Fig. 18. Two-way identical signals are generated by arbitrary waveform generator to connect with two input ports of CMF board, and we select the sinusoidal waves with the magnitude of 0.5 V and the frequency of 5.5 GHz here. Another two ports of CMF board are connected with two channels of digital serial analyzer. Common-mode signals are defined with the voltage sum of two differential microstrip lines [1]. Fig. 19 shows the measured results of common-mode signals received at output ports with CMF board when two input ports are excited with

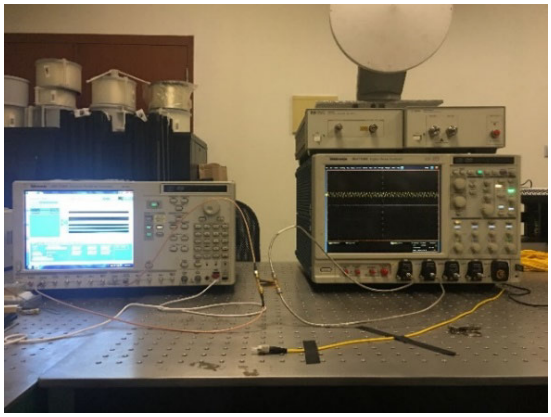

FIGURE 18. Experimental setup in time domain measurement.

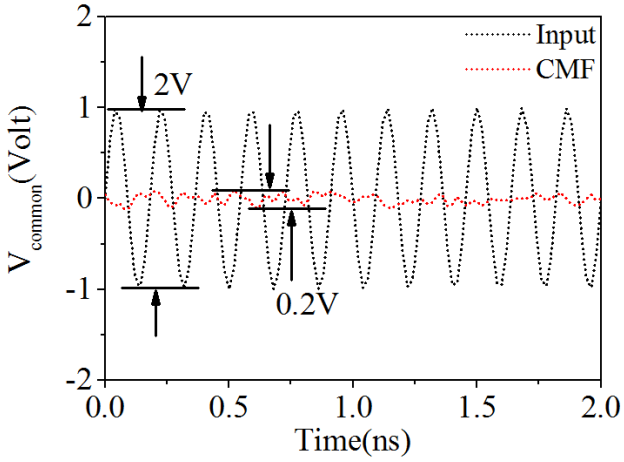

FIGURE 19. The measured results comparison of ideal input common-mode signals and received common-mode signals with CMF board.

ideal sinusoidal waves. The peak-to-peak common-mode signals are 2 V for input ports, while this value is decreased to 0.2 V when the CMF is introduced. 90% amplitude rejection is realized for common-mode noises, which proves the validation of the proposed CMF.

The comparison of this article with previous research is presented in Table 2. Our proposed design has advantages of wide bandwidth and suppression depth for common-mode rejection.

V. CONCLUSION

A common-mode noise suppression filter for high-speed differential signals based on substrate integrated waveguide resonators (SIWR) is presented in this article. The proposed

common-mode filter (CMF) is comprised of cascaded SIWR units. The common-mode noise is decreased more than 25 dB from 4.4 GHz to 14.4 GHz and −15 dB rejection band is obtained in the frequency band of 4.2-17.2 GHz after the CMF is introduced. Moreover, the insertion loss and the group delay in the frequency domain and common-mode noises amplitude suppression and eye diagrams in the time domain are investigated to validate the effectiveness of the proposed CMF. The prototype is fabricated to verify the validity of the proposed structure, and the measurement results show good agreement with the simulation results. Based on these characteristics, the proposed CMF can be a potential candidate for common-mode noises suppression in high-speed circuits.

REFERENCES

[1] G.-H. Shiue, C.-M. Hsu, C.-L. Yeh, and C.-F. Hsu, "A comprehensive investigation of a common-mode filter for gigahertz differential signals using quarter-wavelength resonators," *IEEE Trans. Compon., Packag., Manuf. Technol.*, vol. 4, no. 1, pp. 134–144, Jan. 2014.

[2] T. Sato, S. Ikeda, Y. Hara, K. Yamasawa, and T. Sakuma, "A new multilayered common-mode filter on Ni-Zn ferrite substrate," *IEEE Trans. Magn.*, vol. 37, no. 4, pp. 2900–2902, Jul. 2001.

[3] T. Sato, T. Kokai, A. Moroishi, K. Yamasawa, H. Karasawa, and T. Sakuma, "Mn-Zn ferrite particle/polyimide composite think film and its application to a coupled transmission line common-mode filter," in *Proc. IEEE Int. Symp. Magn.*, Jun. 2002, p. BU4.

[4] K. Yanagisawa, F. Zhang, T. Sato, K. Yamasawa, and Y. Miura, "A new wideband common-mode noise filter consisting of Mn-Zn ferrite core and copper/polyimide tape wound coil," *IEEE Trans. Magn.*, vol. 41, no. 10, pp. 3571–3573, Oct. 2005.

[5] B.-C. Tseng and L.-K. Wu, "Design of miniaturized common-mode filter by multilayer low-temperature co-fired ceramic," *IEEE Trans. Electromagn. Compat.*, vol. 46, no. 4, pp. 571–579, Nov. 2004.

[6] S.-J. Wu, C.-H. Tsai, T.-L. Wu, and T. Itoh, "A novel wideband common-mode suppression filter for gigahertz differential signals using coupled patterned ground structure," *IEEE Trans. Microw. Theory Techn.*, vol. 57, no. 4, pp. 848–855, Apr. 2009.

[7] Z. Zeng, Y. Yao, and Y. Zhuang, "A wideband common-mode suppression filter with compact-defected ground structure pattern," *IEEE Trans. Electromagn. Compat.*, vol. 57, no. 5, pp. 1277–1280, Oct. 2015.

[8] Y.-J. Lu, S.-Y. Chen, and P. Hsu, "A differential-mode wideband bandpass filter with enhanced common-mode suppression using slotline resonator," *IEEE Microw. Wireless Compon. Lett.*, vol. 22, no. 10, pp. 503–505, Oct. 2012.

[9] F. de Paulis, M. Cracraft, C. Olivieri, S. Connor, A. Orlandi, and B. Archambeault, "EBG-based common-mode stripline filters: Experimental investigation on interlayer crosstalk," *IEEE Trans. Electromagn. Compat.*, vol. 57, no. 6, pp. 1416–1424, Dec. 2015.

[10] Q. Liu, S. Connor, C. Olivieri, F. De Paulis, A. Orlandi, M. A. Cracraft, B. Archambeault, and V. V. Khilkevich, "Reduction of EMI due to common-mode currents using a surface-mount EBG-based filter," *IEEE Trans. Electromagn. Compat.*, vol. 58, no. 5, pp. 1440–1447, Oct. 2016.

[11] C. Olivieri, F. de Paulis, A. Orlandi, S. Connor, B. Archambeault, P. Dixon, and M. Khorrami, "Analysis of near-field emissions from common-mode filters based on EBG structures," *IEEE Trans. Electromagn. Compat.*, vol. 59, no. 2, pp. 593–599, Apr. 2017.

[12] C.-H. Tsai and T.-L. Wu, "A broadband and miniaturized common-mode filter for gigahertz differential signals based on negative-permittivity metamaterials," *IEEE Trans. Microw. Theory Techn.*, vol. 58, no. 1, pp. 195–202, Jan. 2010.

[13] F. de Paulis, L. Raimondo, S. Connor, B. Archambeault, and A. Orlandi, "Compact configuration for common mode filter design based on planar EBG," *IEEE Trans. Electromagn. Compat.*, vol. 54, no. 3, pp. 646–654, Jun. 2012.

[14] F. de Paulis, L. Raimondo, S. Connor, B. Archambeault, and A. Orlandi, "Design of a common mode filter by using planar EBG," *IEEE Trans. Adv. Packag.*, vol. 33, no. 4, pp. 994–1002, Nov. 2010.

[15] M. A. Varner, F. de Paulis, A. Orlandi, S. Connor, M. Cracraft, B. Archambeault, M. H. Nisanci, and D. Di Febo, "Removable EBG-based common-mode filter for high-speed signaling: Experimental validation of prototype design," *IEEE Trans. Electromagn. Compat.*, vol. 57, no. 4, pp. 672–679, Aug. 2015.

[16] L. B. Lok, I. D. Robertson, and M. Chongcheawchamnan, "Application of anisotropic EBG for suppressing common-mode resonances in CPW-to-CPS transitions," *Electron. Lett.*, vol. 44, no. 9, p. 584, Jan. 2008.

[17] B.-F. Su and T.-G. Ma, "Miniaturized common-mode filter using coupled synthesized lines and mushroom resonators for high-speed differential signals," *IEEE Microw. Wireless Compon. Lett.*, vol. 25, no. 2, pp. 112–114, Feb. 2015.

[18] P. Vélez, J. Bonache, and F. Martín, "Differential microstrip lines with common-mode suppression based on electromagnetic band-gaps (EBGs)," *IEEE Antennas Wireless Propag. Lett.*, vol. 14, pp. 40–43, 2015.

[19] J. H. Choi, P. W. C. Hon, and T. Itoh, "Dispersion analysis and design of planar electromagnetic bandgap ground plane for broadband common-mode suppression," *IEEE Microw. Wireless Compon. Lett.*, vol. 24, no. 11, pp. 772–774, Nov. 2014.

[20] J. Naqui, A. Fernandez-Prieto, M. Duran-Sindreu, F. Mesa, J. Martel, F. Medina, and F. Martin, "Common-mode suppression in microstrip differential lines by means of complementary split ring resonators: Theory and applications," *IEEE Trans. Microw. Theory Techn.*, vol. 60, no. 10, pp. 3023–3034, Oct. 2012.

[21] H.-R. Zhu and J.-F. Mao, "An ultra-wideband common-mode suppression filter based on S-DBCSRR for high-speed differential signals," *IEEE Microw. Wireless Compon. Lett.*, vol. 25, no. 4, pp. 226–228, Apr. 2015.

[22] J.-X. Chen, W.-J. Zhou, W.-W. Yang, X.-F. Zhang, and Z.-H. Bao, "Wideband tunable common-mode suppression filter based on varactor-loaded slot-ring resonator for high-speed differential signals," *IET Microw., Antennas Propag.*, vol. 11, no. 2, pp. 151–157, Jan. 2017.

[23] H.-H. Chuang and T.-L. Wu, "Suppression of common-mode radiation and mode conversion for slot-crossing GHz differential signals using novel grounded resonators," *IEEE Trans. Electromagn. Compat.*, vol. 53, no. 2, pp. 429–436, May 2011.

[24] M. Kim, "Periodically corrugated reference planes for common-mode noise suppression in high-speed differential signals," *IEEE Trans. Electromagn. Compat.*, vol. 58, no. 2, pp. 619–622, Apr. 2016.

[25] Q. Liu, G. Li, V. Khilkevich, and D. Pommerenke, "Common-mode filters with interdigital fingers for harmonics suppression and lossy materials for broadband suppression," *IEEE Trans. Electromagn. Compat.*, vol. 57, no. 6, pp. 1740–1743, Dec. 2015.

[26] F. Xu and K. Wu, "Guided-wave and leakage characteristics of substrate integrated waveguide," *IEEE Trans. Microw. Theory Techn.*, vol. 53, no. 1, pp. 66–73, Jan. 2005.

[27] Z.-C. Hao, J.-S. Hong, J. P. Parry, and D. P. Hand, "Ultra-wideband bandpass filter with multiple notch bands using nonuniform periodical slotted ground structure," *IEEE Trans. Microw. Theory Techn.*, vol. 57, no. 12, pp. 3080–3088, Dec. 2009.

[28] J. Mao, Y. Xu, R. Zhang, M. Yang, and J. Liu, "Analysis of microstrip discontinuities and their compensation via the finite difference time domain method," in *Proc. Int. Conf. Microw. Technol. Comput. Electromagn. (ICMTCE)*, 2009, pp. 235–237.

[29] A. Fernandez-Prieto, J. Martel-Villagr, F. Medina, F. Mesa, S. Qian, J.-S. Hong, J. Naqui, and F. Martin, "Dual-band differential filter using broadband common-mode rejection artificial transmission line," *Prog. Electromagn. Res.*, vol. 139, pp. 779–797, May 2013.

[30] A. Fernández-Prieto, J. Naqui, F. Medina, J. Martel, F. Martín, F. Mesa, J. Hong, and S. Qian, "Common-mode suppression for balanced bandpass filters in multilayer liquid crystal polymer technology," *IET Microw., Antennas Propag.*, vol. 9, no. 12, pp. 1249–1253, Sep. 2015.

[31] J. S. Hong and M. J. Lancaster, *Microstrip Filters for RF/Microwave Applications*. 2001, pp. 84–89.

[32] C.-L. Wang, G.-H. Shiue, W.-D. Guo, and R.-B. Wu, "A systematic design to suppress wideband ground bounce noise in high-speed circuits by electromagnetic-bandgap-enhanced split powers," *IEEE Trans. Microw. Theory Techn.*, vol. 54, no. 12, pp. 4209–4217, Dec. 2006.

[33] F. Martin, J. Naqui, A. Fernández-Prieto, P. Vélez, J. Bonache, J. Martel, and F. Medina, "The beauty of symmetry: Common-mode rejection filters for high-speed interconnects and band microwave circuits," *IEEE Microw. Mag.*, vol. 18, no. 1, pp. 42–55, Jan./Feb. 2017.

[34] T. Kitazawa and Y. Hayashi, "Analysis of unsymmetrical broadside-coupled striplines with anisotropic substrates," *IEEE Trans. Microw. Theory Techn.*, vol. 34, no. 1, pp. 188–191, Jan. 1986.
[35] A. Attar and M. Joodaki, "Microstrip differential passband filter with high common-mode suppression using periodically loaded stubs and coupled resonators," *J. Eng.*, vol. 2018, no. 4, pp. 242–247, Apr. 2018.

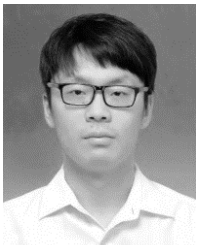

XIAO-LAI LI received the B.S. degree in electrical engineering from Southwest Jiaotong University, Chengdu, China, in 2017. He is currently pursuing the M.S. degree with the Key Laboratory for Information Science of Electromagnetic Waves, Fudan University, Shanghai, China.

His research interests include microstrip antenna design, metasurface design and synthesis, and signal integrity in the high-speed circuits.

GUOMIN YANG (Senior Member, IEEE) received the B.S. degree (Hons.) in communication engineering from the Xi'an University of Technology, Xi'an, China, in 2002, the M.S. degree in electronic engineering from Shanghai Jiao Tong University, Shanghai, China, in 2006, and the Ph.D. degree in electrical and computer engineering from Northeastern University, Boston, MA, USA, in 2010. In 2010, he joined the School of Information Science and Technology, Fudan University, as a Faculty Member, where he is currently a Professor. He has authored 51 journal publications and 50 conference papers. His research interests include antenna miniaturization, magneto-dielectric materials, metamaterials, frequency selective surfaces, microwave wireless power transfer, RF energy harvesting, and inverse scattering problems in electromagnetics.

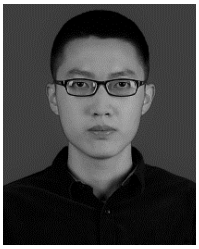

QINZHUO CHEN received the B.S. degree in electrical and information engineering from Northwestern Polytechnical University, Xi'an, China, in 2018. He is currently pursuing the M.S. degree with the Key Laboratory for Information Science of Electromagnetic Waves (MoE), Fudan University, Shanghai, China.

His current research interests include digital coding and programmable metasurfaces, modeling and optimization of metasurfaces, and applications of metasurfaces.